Hussin, Manal, Chan, Tommy, Fawzia, Sabrina, & Ghasemi, Negareh
(2020)
Identifying the prestress force in prestressed concrete bridges using ultrasonic technology.
International Journal of Structural Stability and Dynamics, *20*(10), Article number: 2042014.

https://doi.org/10.1142/S0219455420420146

Identifying the prestress force in prestressed concrete bridges using ultrasonic technology

Manal Hussin [1]
School of Civil Engineering and Built Environment,
Queensland University of Technology
Brisbane, QLD 4000, Australia
manal.hussin@connect.qut.edu.au

Tommy Chan
School of Civil Engineering and Built Environment
Queensland University of Technology
Brisbane, QLD 4000, Australia
tommy.chan@qut.edu.au

Sabrina Fawzia
School of Civil Engineering and Built Environment
Queensland University of Technology
Brisbane, QLD, 4000, Australia
sabrina.fawzia@qut.edu.au

Negareh Ghasemi
School of Information Technology and Electrical Engineering
University of Queensland
Brisbane, QLD 4072, Australia
n.ghasemi@uq.edu.au

Abstract

Monitoring the prestress force (PF) in prestressed concrete bridges (PSCBs) without affecting serviceability has been known as one of the most suitable approaches to achieve a timely decision-making process concerning the health status of the bridges. However, there are currently no accepted nondestructive technologies (NDTs) to evaluate the PF of these bridges, because implementing such a technology in practice is not always feasible due to various difficulties such as the large size of the bridge, tight budget and uncertainties of new technologies.

The Ultrasonic technology is one of the most important NDT that commonly used for measuring the stress state in different materials such as concrete and steel. However, the use of the ultrasonic test to evaluate the PF for prestressed concrete bridge is limited.

In this research, the ultrasonic tests were performed on a prestressed concrete box-girder model to identify the prestressed force according to the acoustoelastic theory. During

[1] Corresponding Author

the tests, the ultrasonic wave was generated using piezoelectric transducers and emitted to the prestressed concrete bridge model. The concrete bridge model was subjected to three different levels of PF, limited to about 30%, 50% and 80% of the ultimate tensile strength. The experimental results showed the increase in prestress force level leads to an increase in the relative change in the wave velocity and the amplitude energy of the ultrasonic wave which proved the acoustoelastic effect theory.

To provide a valid technique to identify the prestress force; different parameters related to the prestressed concrete model (such as the location of the piezoelectric transducers) have been investigated. The present study contributed to the knowledge of the acoustoelastic behaviour of the prestressed concrete and presents the capability of the ultrasonic system in evaluating the stress state in the prestressed concrete bridge.

Keywords: Piezoelectric transducers; prestressed concrete bridge; ultrasonic waves; prestress force; non-destructive testing; box-girder.

1. Introduction

Prestressed concrete bridges (PSCBs) are large, spatially distributed engineered systems that will gradually deteriorate with time if they cannot be managed and maintained properly. Considering their invaluable societal functionality, the long-term health management of these bridges is just as important as their design and construction. The prestress force (PF) level in PSCBs is one of the most important parameters in their construction and service life. However, it is hard to be measured via traditional methods such as virtual inspection due to the complexity of the PSCB.

Non-destructive tests are important inspection method since they do not affect the serviceability or the future life of the structure [1]. Among the current methods of nondestructive technology (NDT), ultrasonic technology has received the most researchers' attention. Ultrasonic waves, which propagate through materials with sufficient depth, have shown great potential as an effective measurement approach [2]. Ultrasonic stress evaluation techniques are based on the "acoustoelastic" effect, which refers to the relationship of stress and relative variation in wave velocity of the elastic wave propagation in a structure undergoing static elastic deformation [3, 4].

The principles of acoustoelastic effect and ultrasonic wave velocity measurements have been used in laboratory and field tests in many engineering applications. The residual stresses in welded steel plates and railroad rails have been measured by Leon-Salamanca and Bray [5] and Tanala et al. [6]. While Hirao et al. [7] and Manchem et al. [8] measured the stress level in bars and multiwire strands. Clark et al. [9] have developed Noncontact electromagnetic-acoustic transducer (EMAT), which operates based on acoustoelastic effect, for measuring live load stresses in highway bridges. The researchers focused on the use of the Rayleigh waves generated on the surface of an I-beam to measure the relatively low live stresses (less than 14 MPa) typically experienced by bridge girders [9]. The research demonstrated that the acoustoelastic effect could be used effectively to measure the applied stress in a four-point bending test in the lab. Clark et al. [10] demonstrated that the EMAT based on the acoustoelastic behavior could be constructed to perform these measurements successfully under field conditions. Popovics and Popovics [11] studied the effect of stresses level on ultrasonic tests experimentally using concrete cylinders subjected to gradual load increment. The experimental results showed that the wave velocity and the stress level are independent.

Generally, the ultrasonic technique is one of the most practical and attractive approaches that has been used in the PF identification area, as a large area of a structure can be evaluated using a single transducer. Hence, it avoids the time-consuming point-by-point scanning required for conventional inspection methods. Most of the literatures focused on prestressed identification only on either steel bridges, concrete specimens or prestressed concrete with exposed tendons, where the transducers and the receivers attached at the ends of the steel tendons and PF can be calculated directly. While in reality, most of the PSCBs are designing and constructed with embedded tendons. Therefore, this research is aiming to extend the current knowledge in prestress force identification to the PSCBs with embedded unbonded tendons.

The capability of the piezoelectric transducers in generating ultrasound waves regardless of the type of medium makes them a potential candidate for prestressing detection on the concrete surface or on the steel tendons. Two ultrasonic piezoelectric transducers (transmitter and receiver) were attached on the concrete surface to send and receive the ultrasound wave. The stresses developing at the concrete surface were used for the inverse calculating of the PF applied on the steel tendons. The relative change in the ultrasonic wave velocity was studied to determine the PF in the prestressed concrete model according to acoustoelastic theory. Another ultrasonic wave parameter such as the change in delivered energy had been also studied during the experimental tests to determine the feasibility of using wave velocity to evaluate the PF of the PSCBs, and finally to provide a non-invasive evaluation technique to identify the PF of the PSCBs.

2. Acoustoelastic theory

Hughes and Kelly [12] developed equations based on the Murnaghan's theory to represent the acoustoelastic effect in isotropic materials for finite deformations and nonlinear elasticity [13]. Equations (2.1-2.5) show the longitudinal and shear wave velocities of ultrasonic wave along the directions of an isotropic solid undergo uniaxial stress in x-direction. In this article the prestressed concrete bridge has been used as an example of isotropic solid as shown in Figure 1.

$$\rho V_{11}^2 = \lambda + 2G + \frac{\sigma_{11}}{3K}\left[2\ell + \lambda + \frac{\lambda+2G}{G}(4m + 4\lambda + 10G)\right] \tag{2.1}$$

$$\rho V_{12}^2 = \rho V_{13}^2 = G + \frac{\sigma_{11}}{3K}\left[m + \frac{\lambda n}{G} + 4\lambda + 4G)\right] \tag{2.2}$$

$$\rho V_{22}^2 = \rho V_{33}^2 = \lambda + 2G + \frac{\sigma_{11}}{3K}\left[2\ell - \frac{2\lambda}{G}(m + \lambda + 2G)\right] \tag{2.3}$$

$$\rho V_{21}^2 = \rho V_{31}^2 = G + \frac{\sigma_{11}}{3K}\left[m + \frac{\lambda n}{4G} + \lambda + 2G)\right] \tag{2.4}$$

$$\rho V_{23}^2 = \rho V_{32}^2 = G + \frac{\sigma_{11}}{3K}\left[m - \frac{\lambda+G}{2G}n - 2\lambda\right] \tag{2.5}$$

[Figure 1. The direction of wave propagation on the surface of the prestressed concrete bridge model]

In these Equations, V_{ij} is the ultrasonic wave velocity, subscript i is wave direction and j is the stress direction, σ_{11} is stress calculated according to Equation (3.8) as will be explained later, ρ is the material's density, m, n and ℓ are the Murnaghan's elastic constants, λ is the Lamè first elastic constant, G is the dynamic shear modulus and K is the volumetric modulus and can be calculated using Equation (2.6). Equations (2.1-2.5) can be linearized [1, 14], which result in Equation (2.7).

$$K = \lambda + \frac{2}{3}G \tag{2.6}$$

$$\frac{V_{ij}^{\sigma} - V_{ij}^{0}}{V_{ij}^{0}} = A_{ij}\sigma_{11} \tag{2.7}$$

In Equation (2.7), V_{ij}^{σ} and V_{ij}^{0} are the wave velocities in the prestressed concrete model with and without PF respectively, and A_{ij} is the acoustoelastic constant. Equation (2.7) represented the acoustoelastic theory and shows the relationship between the change in the ultrasonic wave velocity and the stress developed on the concrete surface due to apply PF on the steel tendons.

3. Experimental tests and model preparation

The PF was evaluated through experimental tests using ultrasonic technology and a prestressed concrete box-girder model. This section describes the model preparation, materials properties, test prototyping and other test configurations used as part of the study. The effectiveness of the proposed method has been studied under different conditions as will be explained later.

3.1 Box-girder description

A scaled-down physical model of a six-meter-long continuous concrete bridge represents a typical prestressed concrete box girder bridge [15, 16]. The model was single-span, prestressed, post-tensioned with a box-girder cross-section, equipped with various sensors to continue monitoring strain, deflection, displacement, acceleration and support reaction forces. The model was symmetrical about the centre point, which divided the whole model length into two equal spans of three meters each, 440 mm in depth and 1000 mm in width as shown in Figure 2.

[Figure 2. Cross-section of the lab model (All dimensions are in mm) [15, 16]]

Longitudinal and shear reinforcement were provided to the box-girder according to ACI guidelines [17], as shown in Figure 3. The beam was post-tensioned concentrically with two parabolic tendons, symmetrical about the centerline, each tendon consisted of seven wires with nominal diameters of 15.2 mm. To anchor the tendons, wedge barrels and two steel plates (85 mm × 150 mm × 20 mm) were used at the ends of the tendons as shown in Figure 4.

[Figure 3. Reinforcement details of the lab model [15, 16]]

[Figure 4. End anchorages of strand [15, 16]]

3.2 Construction of the lab model

The model was casted in three sequences, the minimum duration between two sequences was 10 days. For each sequence, the model was moist-cured for seven days by covering it with saturated burlap and plastic sheeting. Beyond eight days, the model was kept in laboratory air. Plywood formwork with timber supports have been used during the construction of the model, as shown in Figure 5.

[Figure 5. Formwork used during the construction [15, 16]]

Stage 1 (Bottom Slab)

The bottom slab was the first part of the box-girder model that was constructed. It was an 80 mm thick reinforced concrete slab connected to the webs along its longer edge. Sufficient reinforcements were provided across the joint to avoid cracks and to allow the model to behave as a single unit. Figure 6 shows Stage 1 of the model construction before and after concreting.

[Figure 6. Construction of the model, Stage 1, (a) Before concreting, (b) After concreting]

Stage 2 (Webs)

To improve the bond between the surface of the bottom slab and the webs of the box-girder, the surface of the hardened concrete was chipped. The duct of the prestressing strand and the longitudinal rebar were tied to the vertical reinforcement as shown in Figure 7.

[Figure 7. Construction of the model, Stage 2 (webs), (a) Formwork for webs (b) Concreting the webs, (c) After removing formwork]

Stage 3 (Top Slab)

Same procedures used during Stage 2 were repeated to construct the top slab of the box- girder. To improve the bonding between the two surfaces (the webs and the top slab), the surfaces of the construction joints were made rough. Figure 8 shows Stage 3 of the construction model.

[Figure 8. Construction of the model, Stage 3 (top slab)
(a) Reinforcing and formwork, (b) Top slab after concreting, (c) Completed model]

The tendons were unbonded and encapsulated within a protective sleeve and placed adjacent to the concrete. At each end of each tendon, there was an anchorage assembly firmly fixed to the surrounding concrete. The box-girder is built up with end diaphragm to resist torsional distortions and reduce the deflection resulting from concentrated loading due to support condition. The end diaphragm was made of steel cross frame (5 mm thick, 50 mm × 50 mm) located at the support locations. and it was tightly fitted to the model as shown in Figure 8, (c). The box-girder was located on two half-cylindrical steel supports, leaving a simply supported beam with a 5.8 m long span. Once the concrete had been casted, the steel unbonded tendons were tensioned by pulling the tendon ends through the anchorages using a hydraulic mono jack. The other end of the strand was anchored to the concrete using a wedge barrel and steel plate. When the required concrete strength was achieved, the stressing or post-tensioning process was started to produce the required tension in the strands. Figure 9 shows the prestressing equipment, process and load cell reading during tensioning. More elaboration about the construction procedures can be found in Hussin [16] and Pathirage [15].

[Figure 9. Process of applying the prestressed force, (a) Prestressing equipment and process, (b) Load cell reading during tensioning]

3.3 Ultrasonic measurement system

In this section, a brief description of the developed ultrasound system is presented. To excite the transmitter, a signal generator (Agilent 33500B waveform generator) was utilised to generate a sinusoidal signal with a fundamental frequency 44 kHz. A high- performance 4-channel RIGOL digital oscilloscope (RIGOL DS 1204B) was used to measure and capture the voltage across the receiver. Compared to the available systems for measuring ultrasonic wave response, the system benefits from lower cost and simple structure and controls. The piezoelectric transducers (PZT) are the most important part of the ultrasonic system made with piezoelectric material. The piezoelectric materials possess advantages of high sensitivity, high renounce frequency, and high stability. These advantages make the piezoelectric traducers potential candidate for detecting any change in the stress, temperature, and cracks of the concrete structure [18]. Therefore, these sensors have been widely used in stress monitoring in the concrete structure [19-21].

In the experimental tests, two piezoelectric transducers were used to generate and receive the ultrasonic waves respectively. Coupling between the transducers and the surface is necessary; otherwise, the acoustic impedance mismatch between air and solids will be large and nearly all the energy would be reflected, and a small portion of it would be transmitted through the test [22]. Therefore, a thin layer of ultrasonic gel was used and applied between the transducers and the tested surface.

3.4 Material properties of the constructed model

After leaving the concrete of the model to gain the desired strength, numbers of tests such as compressive strength, density, and modulus of elasticity were performed on the eighteen concrete cylinders' samples prepared in parallel with the casting of the two slabs and webs. Table 1 shows the material properties of each part of the model.

[Table.1 Materials properties of the tested model]

3.5 Test prototyping

This research is being developed to identify the effective PF from the inverse calculation of stress developed on the concrete surface due to the applied PF on the steel tendons as will be explained later. The piezoelectric ultrasonic transducers are mounted to the concrete surface and excited by a high-frequency (44 kHz) acoustic signal. The wavelength of this signal is small enough to be sensitive to any developing stress on the concrete surface due to the PF applied to the steel tendons. Acoustoelastic constants (A_{ij}) is a very important parameter in PF identification, therefore; calibration tests have been conducted in three different locations on the concrete surface to calculate this constant.

Zero-stress state has been considered as the base data, in order to compare with other results due to changing the stress state (applying the PF levels). Three prestressing force levels (shown in Table 2) were experienced on the box-girder (PF1, PF2, and PF3) due to tensile force applied to the steel tendons of the model. The applied tensile forces on the steel tendons were limited to about 30%, 50% and 80% of the ultimate tensile strength (UTS) which is about 261 kN of the tested tendons. Therefore, with the previous process, we obtained the same stress distribution as in site conditions.

[Table.2 PF levels applied to the model]

The relative change of the wave velocity was determined from the travel time of the ultrasonic waves from the transmitter to the receiver. The transmitter and the receiver were attached to the surface of the concrete, and the distance between them was adjusted to 30 cm.

This propagation distance has been chosen after running numbers of ultrasonic tests. At this distance (30 cm), the received voltage had a better resolution and highest amplitude.

Eight transducers and eight receivers were fixed on the concrete surface of the box-girder model during the experimental program in different locations. Two test setups were used for measuring the relative changes in the wave velocity achieved for different prestressed loads. These two setups were in the compression stress zone of the box-girder under the neutral axis (NA), because at this zone the effect of the PF would appear very clear through consolidating the model which is the main purpose of using the prestress concrete technique. Therefore, most of the microcracks and the voids created during the construction of the model will be either reduced in size or closed perfectly and resultant in a more homogenous consolidating zone.

The first experimental test setup was performed at the web section, the transmitters and the receivers placed at three different locations. These locations were chosen close to the tendon's location. For the second experimental test setup, the transmitters and the receivers placed under the bottom slab of the box-girder and they aligned along the centerline of the model. The purpose of adopting different experimental setups was to find out the most efficient locations to identify the PF. The change in the wave velocity was determined from the travel time of the waves from the transmitter to the receiver attached on the surface of the concrete model.

3.6 Stress state analysis of the box-girder

As the transducers and the receivers were attached on the concrete surfaces, the relative change that developed in the wave velocity was caused by changes in the stress states at the concrete surface due to the application of different PF on the steel tendons (assuming the stress due to the dead weight is constant). Figure 10 illustrates a typical section of the prestressed box-girder used in the experiment with an eccentricity (e_B) from the NA. For the section shown in Figure 10, under working load moment (M_w), the following Equation (3.8) is used to calculate the stress and can be written by virtue of the principle of superposition adapted from the Australian Standard-AS 3600-2009 (Standard, 2009)

[Figure 10. Stress distribution in a prestressed box-girder beam under working load moment adapted from the Australian Standard AS 3600-2009 [23]]

$$f_{cB} = \frac{PF}{A} + \frac{PF * (-e_B) * (-Y_B)}{I} + \frac{M_w * (-Y_B)}{I} \quad (3.8)$$

In Equation (3.8), f_{cB} is the compressive stress (σ_{11}), PF is the prestressed force applied, A is a cross-section area of the box-girder, I is the 2nd moment of area, e_B is the eccentricity of the tendons and Y_B is distance between the receivers' location and the NA and (M_w) is the working load moment.

4. Results and discussion

In this research, the wave velocities were calculated by measuring a delay that was obvious in the captured signals compared to the Zero-stress state (reference signal) results using the cross-correlation method [4, 24]. More elaborations about the cross-correlation method used to calculate the delay between two signals can be found in Hussin [16].

The reference velocity V_0 in the Zero-stress state was equal to 3726.66 m/s. This value corresponds to the phase velocity of zero symmetric modes at the frequency of f=44 kHz calculated using WAVESCOPE software as shown in Figure 11. The software was developed at the University of South Carolina College of Engineering and Computing in connection with LAMSS (Laboratory for Active Materials and Smart Structures).

[Figure 11. The ultrasonic wave phase velocity of the box-girder determined using WAVESCOPE software]

To provide a valid technique to identify the PF in the PSCBs, different parameters related to the prestressed concrete model such as the receivers' position have been investigated as will be explained in the next two sections.

4.1 Effect of the receiver's position (Webs)

Three different locations under the NA (compressive stresses part) were marked on the left-hand side of the girder (close to the tendon's position inside the prestressed box-girder model). Figure 12 shows the locations of the PZT receivers attached at the web slab of the box-girder. As mentioned previously, the distance between the transmitter and the receiver was fixed to be 30 cm. Therefore, any change in the velocity of the ultrasonic wave was due to applied PF in the steel tendons. Figures 13 and 14 shows the experimental setup at the web slab of the box-girder and examples of the normalized signals received by receiver RW1 under different levels of PF respectively.

[Figure 12. Positions of the receivers RW1, RW2, and RW3 on the web slab of the model (Note: the dimensions are not to scale)]

[Figure 13. Test set-up at the web part of the box-girder]

[Figure 14. An example of signals received by RW1 with respect to different PF, with a close-up of the first part of the signal]

After processing and examining all the signals received by the receivers (RW1, RW2, and RW3) attached at the web of the model, the relative changes in the wave velocity was calculated using the cross-correlation method. Figure 15 shows the relationship between the relative change in the wave velocity and the stresses at the web of model. These data correspond to three acoustoelastic tests in three different locations and covered the same stress distribution as in site conditions starting from PF1: low prestressed level, PF2: medium prestressed level and PF3: high prestressed level.

[Figure 15. Relative changes in the wave velocity as a function of applied stress in the web slab of the model]

In Figure 15, it can be observed that there was a minor increase in the relative change of the wave velocity (about 0.23%) when the PF changed from PF0 to PF1, which caused a small increase in the velocity of the ultrasonic wave. This behavior can be attributed to the small reduction in the size of the flexural microcrack which is usually created in the negative moment area (tensile zone). This type of microcrack happens during the construction before the PF is applied due to many reasons such as self-weight of the box-girder. The crack width can be between 0.1 and 0.2 mm [25], as a result, they will create an imperfect contact interface in the surface of the box-girder. Further, it can happen in or near the segment joints such as (bottom and web slabs) [25]. Some of these microcracks occur within a few hours (first six hours) after the placement and compaction of concrete. However, most of these microcracks will be closed after the PF is applied, while others remain open even after the PF has been applied [25]. Therefore, after applying the PF1, the PF was not enough to close all the voids and the micro cracks. Thus, the effect of the prestressing was not yet clear.

After applying the PF2 level, the wave velocity increased by around 50%. At this level of PF, the effect of the PF appeared very clear. Most of the voids and microcracks sizes were reduced or completely closed by compressing the model which is the main purpose of using the prestressed concrete. Conversely, after applying PF3 there was a slight increase in the relative change of the wave velocity, which can be attributed to the fact that the box-girder had already reached the desired compression state at this prestressed level. From Figure 15 the measured trend exhibits a nearly perfect linear relationship between the stresses developed in the concrete surface due to the application of PF (at the web) and the relative change in the wave velocity and monotonic suggesting that linear curves can be fitted using the least square regression to calculate the acoustoelastic constant A_{ij}.

This finding is consistent with other scholars' research results [26], and acoustoelastic theory, which demonstrated that the proposed method is suitable for the PF evaluation of the prestressed concrete members. The increase in wave velocity was due to the increase in the compressive stress and hence modulus of elasticity and the density of the concrete surface of the box-girder, resulting from PF applied to the tendons. To calculate the stress from the acoustoelastic Equation 2.7, the acoustoelastic constant (A_{ij}) needed to be determined from the slopes of Figure 15. After governing the data of the previous experimental setup, it was found that A_{ij} is equal to 2.6×10^{-7} (the average value for three tests in three different locations). This value has been used in all calculations presented in this paper. The stress value calculated using Equation 2.7 was employed for the inverse calculation of the PF using Equation 3.8, as described previously. Figure 16. Shows the values of the real PF applied during the experiment and the PF calculated at receivers RW1, RW2, and RW3 from the ultrasonic data.

[Figure 16. PF calculated from the ultrasonic wave data at the receiver's locations (web part results)]

From Figure 16, it can be observed that PF2 and PF3 were successfully identified in the receiver RW2 with a reasonable percentage of error. This can be attributed to the location of this receiver on the web slab of the box-girder close to the tendon's location with reasonable distance from the NA. Meanwhile, receiver RW1 gave the second good calculation error in PF2 and PF3. Conversely, the PF1 and PF2 calculated in the receiver RW3 were roughly underestimated compared with the other receiver's' data. That can be attributed to the location of receiver RW3 near the joint between the web and the bottom slab. This position usually has high percentage of microcracks as explained previously, however, some of these microcracks remained open even after applying the PF, which directly affected the results. It was observed that the PF2 and PF3 identifications were better than PF1, which can be attributed to the fact that changing the wave velocity highly depends on the change of the material properties such as density and modulus of elasticity. At this prestress level (PF1), the change was not high enough to be detected; therefore, no significant results were observed.

4.2 Effect of receivers' position **(Bottom slab)**

The test was also performed on the bottom slab under the box-girder. Five transmitters and five receivers were attached along the centre line of the box-girder. Figure 17 shows the second developed experimental prototype under the bottom slab of the box girder and the locations of the transmitters and the receivers. The same ultrasonic system used in the web part was also used in this experimental prototype. The same procedure for applying the PF and calculating the relative change in the wave velocity was repeated for this experiment.

[Figure 17. Experimental prototype with transducers placed under the bottom slab of the box-girder and the positions of the transmitters (TB) and the receivers(RB) under the bottom slab of the girder. (Note: the sketch is not to scale)]

Figure 18 shows the relative change in the wave velocity as a function of stresses developed in the receiver locations under the bottom slab of the box-girder. The experimental results conducted from the five receivers attached at the bottom slab of the box-girder indicated two acoustoelastic behaviours, as shown in Figure 18. The first expression observed for RB1 and RB2 and RB5 in Figure 18 represents an increase in the relative change in the wave velocity with an increase in the compressive stress due to the application of PF. This behaviour was similar to the response of the ultrasonic transducers at the web part of the model. Different behaviour indicated for RB3 and RB4 as shown in Figure 18. The behaviour started after applying PF2, where the relative change in the wave velocity reduced significantly and continued reducing even after applying PF3.

[Figure 18. Relative change in the wave velocity as a function of applied stress of the receivers]

This change in the behaviour of the ultrasonic wave in the receivers attached under the bottom slab of the box-girder can be attributed to the off-centre location of the prestressing steel, which caused a cambered shape to the box-girder before applying the live load. The cumulative results at this part are directly related to the wave velocity at zero stress. However, at this stress level (zero) the deflection was about 5 mm downward calculated according to Equation 4.9 [27], which prevented the transducers and the receivers from aligning correctly. Hence, the receivers did not catch the signal appropriately in the middle part of the box-girder. After applying the PF, the same position was under camber, which was due to subscription the upward displacement from the downward displacement calculated according to Equation 4.10 [27]. Therefore, the receivers RB3 and RB4 were attached in unstable places and could not receive the signal appropriately. Therefore, the signals detected at these two positions have been excluded from the final calculation. This drawback might be overcome in real prestressed concrete bridges due to applying service and a live load.

$$deflection\ (down\ ward\ ) = \frac{WL^4}{384El} \tag{4.9}$$

$$deflection\ \ (upward\ )\ = \frac{ML^2}{8EI} \tag{4.10}$$

Where, W is the dead load, L is the length of the box-girder, E is the modulus of elasticity, I is the 2nd moment of Area and M is the moment due to PF. The same procedures were used to identify the PF at receivers RB1, RB2 and RB5. Figure 19 shows the final identification of the PF from the ultrasonic data. According to the experimental results of this section, there was a direct relationship between the receiver positions and stress monitoring of the prestressed concrete box-girder. However, the ultrasonic technology failed to identify PF1 in all the receivers attached under the bottom slab. The PF was successfully identified in RB1, RB2, and RB5 for PF2 and PF3 with an acceptable percentage of error: less than 10%, similar to the results detected at the receivers attached at the web slab of the box-girder.

[Figure. 19 Calculated PF from the ultrasonic wave data at the receiver's locations (under the bottom slab of the girder results)]

5. Wave amplitude energy

During the experimental program, it was observed that the amplitude energy of the ultrasonic signal was also affected when the PF changed as showed previously in Figure 14. Therefore, to quantify such a variation, the signals detected at the web slab of the box-girder have been used for this analysis. However, due to limited information about this phenomenon (the effect of PF on the amplitude energy of the ultrasonic wave); the method developed by Aggelis and Shiotani [28] about the effect of the inhomogeneity parameters in cementitious material on amplitude energy of the ultrasonic wave has been followed in this research. The method started by calculating the total energy of each waveform as the area under the rectified signal envelope using MATLAB as shown in Figure 20. To present the percentage of the energy transmitted through the surface of the prestressed concrete with different PF levels, the area under the envelope was then divided by the energy achieved as a response of the face-to-face transducers demonstrated in Figure 21.

[Figure 20. Received signal and the created energy envelope to calculate the area under the signal]

[Figure 21. Measurement of the transmitted (face-to-face contact)]

Figure 22 shows the results of the percentage of the waveform energy as a function of stresses with different PF levels respectively. In Figure 22, it is obvious that the waveform energy of the ultrasonic signal increases with increases in the PF level. This can be attributed to the fact that after applying the PF, most of the microcracks, voids, and inhomogeneity in the box-girder created due to the dead load or during the construction have been closed and resulted in more homogenous section. Therefore, the ultrasonic signal is propagating quite more easily and smoothly through the surface of the prestressed concrete model after applying the PF. According to the experimental results, it can be concluded that the change in the voltage measured across the receiver can be used as an indication for PF level reduction inside the prestressed concrete structure. However, this phenomenon still needs to be addressed further as the literature about this topic is still limited to cementitious materials only. Therefore, more research needs to be conducted for prestressed concrete to develop final theory for this parameter.

[Figure 22. Waveform energy vs. stresses developed due to applying PF]

6. Conclusions

The effectiveness of the ultrasonic technology in the detection of PF on prestressed concrete box-girder bridge model was studied experimentally. Several experimental tests were conducted under different test conditions such as changing the locations of the piezoelectric transmitter and receiver. The results showed that the change in the applied PF level on the steel tendons can be detected as a change in the ultrasonic wave velocity.

The experimental results revealed that the PF2 (1.58 MPa) and PF3 (2.1 MPa) levels have been identified with very good accuracy (less than 10% error) in most of the receivers such as; RW1, RW2, RB1, RB2, and RB5. These ranges of the applied PF were in usual range proposed for real structure (between 1 MPa and 3 MPa) according to Khan and Williams [29]. Therefore, the finding of this research demonstrates the effectiveness of the proposed method to identify the PF of the PSCBs and to be successfully used in the field applications. However, scattering in the experimental results were observed in some experimental tests, RW3, RB3, RB4 due to the receiver locations at the joints between the bottom slab and the web, and at the middle part of the bottom slab. Therefore, it is very important to avoid these two places. Scattering in the experimental results was also observed in the PF1 (about 0.95 MPa). However, PF1 is not in the range of prestressing level for the real structure as mentioned before. Thus, this technology is still very effective in identifying the PF in the real PSCBs.

In addition, it has been observed that the change in the PF level will influence the amplitude energy of the ultrasonic wave during the experimental program. Results showed that the amplitude of the received signal increases if larger PF is applied. Therefore, this parameter can also be used to monitor the PF level during the life service of the bridge. Finally, relationships between the change in the wave velocity, amplitude energy of the ultrasonic wave and the PF level were evaluated.

Results showed that these wave's parameters seem to be correlated to an associate of the PF level. Therefore, this research supported the knowledge on the acoustoelastic behavior of the prestressed concrete and presents an advanced method for evaluation of the PF level in the field applications.

7. Acknowledgments

The authors would like to thank, Queensland University of Technology (QUT) and Australian Research Council (ARC Discovery Project) (Grant No. DP130104133) for providing support and funding to carry out the work reported in this paper. The authors would also like to express their gratitude to Pathirage Thisara Shamane, Ziru Xiang and whosoever had contributed to their work either directly or indirectly.

8. References

1. Bompan, K. F. and V. G. Haach, *Ultrasonic tests in the evaluation of the stress level in concrete prisms based on the acoustoelasticity.* Construction and Building Materials, 2018. **162**: p. 740-750.
2. Li, J. He, J. Teng, et al., *Internal Stress Monitoring of In-Service Structural Steel Members with Ultrasonic Method.* Materials, 2016. **9**(4): p. 223.
3. Payan, C., V. Garnier, J. Moysan, et al., *Determination of third order elastic constants in a complex solid applying coda wave interferometry.* Applied Physics Letters, 2009. **94**(1): p. 011904.
4. Pei and K. Demachi, *Numerical simulation of residual stress measurement with acoustic wave.* EJ Adv Maint Jpn Soc Maintenol, 2010. **2**: p. 160-167.
5. Leon-Salamanca, T. and D. F. Bray, *Residual stress measurement in steel plates and welds using critically refracted longitudinal (LCR) waves.* Research in Nondestructive Evaluation, 1996. **7**(4): p. 169-184.
6. Tanala, E., G. Bourse, M. Fremiot, et al., *Determination of near surface residual stresses on welded joints using ultrasonic methods.* NDT & E International, 1995. **28**(2): p. 83-88.
7. Hirao, M., H. Fukuoka, H. Toda, et al., *Non-destructive evaluation of hardening depth using surface-wave dispersion patterns.* Journal of Mechanical Working Technology, 1983. **8**(2–3): p. 171-179.
8. Manchem, L. D., M. N. Srinivasan, and J. Zhou. *Analytical Modeling of Residual Stress in Railroad Rails Using Critically Refracted Longitudinal Ultrasonic Waves With COMSOL Multiphysics Module*. in *ASME 2014 International Mechanical Engineering Congress and Exposition*. 2014. American Society of Mechanical Engineers.
9. Clark, P. Fuchs, and Schaps, *Fatigue load monitoring in steel bridges with Rayleigh Waves.* Journal of Nondestructive Evaluation, 1995. **14**(3): p. 83-98.

10. Clark, P. A. Fuchs, M. G. Lozev, et al., *Ultrasonic Measurement of Stress in Bridges*, in *Nondestructive Characterization of Materials VIII*, R. Green, Jr., Editor. 1998, Springer US. p. 481-486.
11. Popovics, S. and J. S. Popovics, *Effect of stresses on the ultrasonic pulse velocity in concrete.* Materials and Structures, 1991. **24**(1): p. 15-23.
12. Hughes, D. S. and J. L. Kelly, *Second-Order Elastic Deformation of Solids.* Physical Review, 1953. **92**(5): p. 1145-1149.
13. Murnaghan, F., *Finite deformation of an elastic solid.* New York, 1952.
14. Lillamand, I., J.-F. Chaix, M.-A. Ploix, et al., *Acoustoelastic effect in concrete material under uni-axial compressive loading.* NDT & E International, 2010. **43**(8): p. 655-660.
15. Pathirage, T. S., *Identification of prestress force in prestressed concrete box girder bridges using vibration based techniques*. 2017, Queensland University of Technology.
16. Hussin, M. K., *Identification of prestress force in prestressed concrete box girder bridges using ultrasonic technology*, in *School of Civil Engineering & Built Environment*. 2018, Queensland University of Technology Australia p. 201.
17. ACI committee 318, A. C. I., *Building Code requirements for Structural Concrete (ACI 318-08) and Commentary*. 2008: American Concrete Institute.
18. Baoguo, H., X. Yu, and J. Ou, *Self-sensing concrete in smart structures.* 2015.
19. Kevin, K. T. and W. Liangsheng, *Smart piezoelectric transducers for in situ health monitoring of concrete.* Smart Materials and Structures, 2004. **13**(5): p. 1017.
20. Wen, Y., Y. Chen, P. Li, et al., *Smart Concrete with Embedded Piezoelectric Devices: Implementation and Characterization.* Journal of Intelligent Material Systems and Structures, 2006. **18**(3): p. 265-274.
21. Yi, M. and Y. Weijian, *Application of a PVDF-based stress gauge in determining dynamic stress–strain curves of concrete under impact testing.* Smart Materials and Structures, 2011. **20**(6): p. 065004.
22. Claudio, N., *Guided wave monitoring of prestressing tendons*. 2010, UC San Diego: b6940590. Retrieved from: https://escholarship.org/uc/item/0xd0t7q6.
23. Standard, A., *Reinforced and Prestressed Concrete: Analysis and Design with Emphasis on Application of AS3600-2009 2nd Edition,*, in *prestressed concrete* 2009.
24. Stähler, S. C., C. Sens-Schönfelder, and E. Niederleithinger, *Monitoring stress changes in a concrete bridge with coda wave interferometry.* The Journal of the Acoustical Society of America, 2011. **129**(4): p. 1945-1952.

25. Podolny, W., *The cause of cracking in post-tensioned concrete box girder bridges and retrofit procedures.* Journal of the Prestressed Concrete Institute, 1985. **30**(2): p. 82-139.

26. Washer, G. A., *The acoustoelastic effect in prestressing tendons*. 2001, The Johns Hopkins University.

27. Hibbeler, R. C., *Structural analysis*. 1995: Simon & Schuster Books For Young Readers.

28. Aggelis, D. G. and T. Shiotani, *Effect of inhomogeneity parameters on wave propagation in cementitious material.* ACI materials journal, 2008. **105**(2): p. 187.

29. Khan, S. and M. Williams, *Post-tensioned concrete floor*. 1995, Great Britain CRC press

Tables

Table.1 Materials properties of the tested model

Property	Section		
	Top slab*	*Webs**	*Bottom* slab*
Compressive strength (MPa)	*47.43*	*49.89*	*53.12*
Modulus of elasticity (GPa)	*30.6*	*31.38*	*32.38*
Density (kg/m^3)	*2320*	*2320*	*2320*

**Average of six samples*

Table.2 PF levels applied to the model

PF level	*Tendon 1 (kN)*	*Tendon 2 (kN)*	*PF Apply (kN)*
PF0	*0*	*0*	*0*
PF1	*85*	*86*	*171*
PF2	*142.402*	*141.607*	*284.009*
PF3	*186.16*	*192.133*	*378.29*

Figures

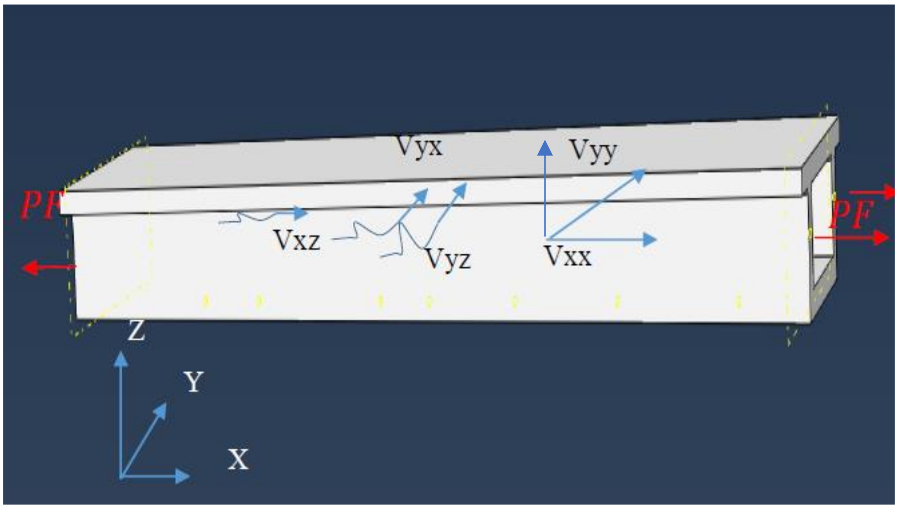

Figure 1. Direction of wave propagation on the surface of the prestressed concrete bridge model

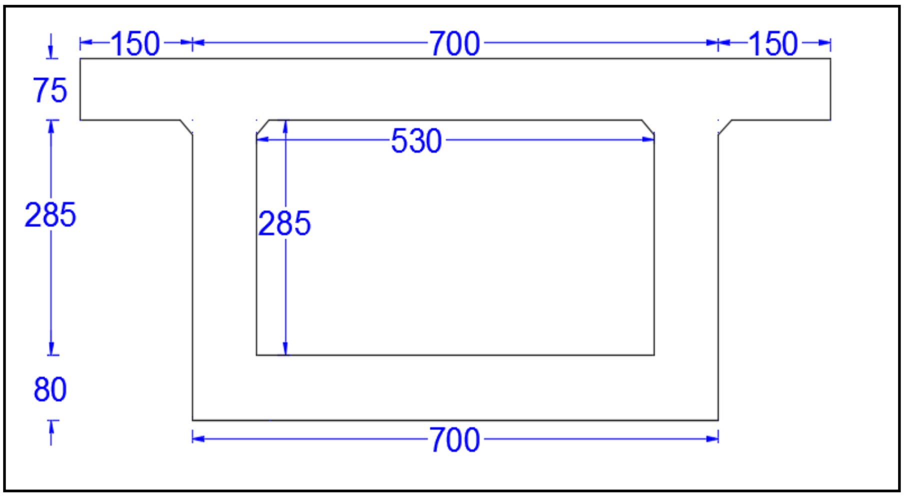

Figure 2. Cross-section of the lab model (All dimensions are in mm)[15, 16]

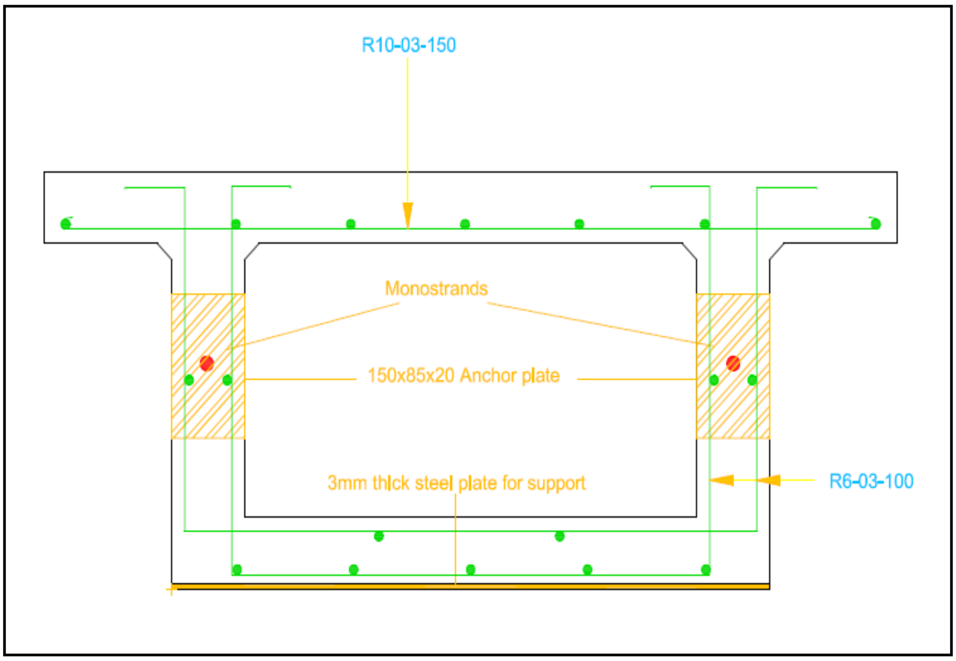

Figure 3. Reinforcement details of the lab model (Front view)[15, 16]

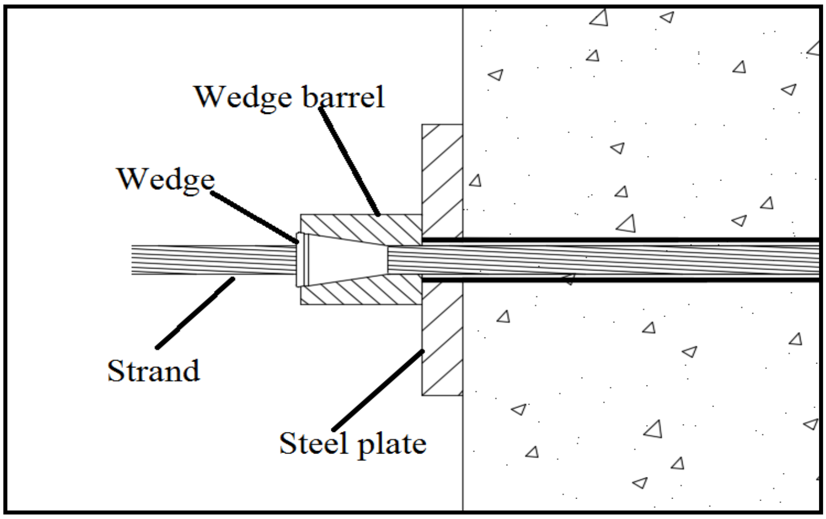

Figure 4. End anchorages of strand [15, 16]

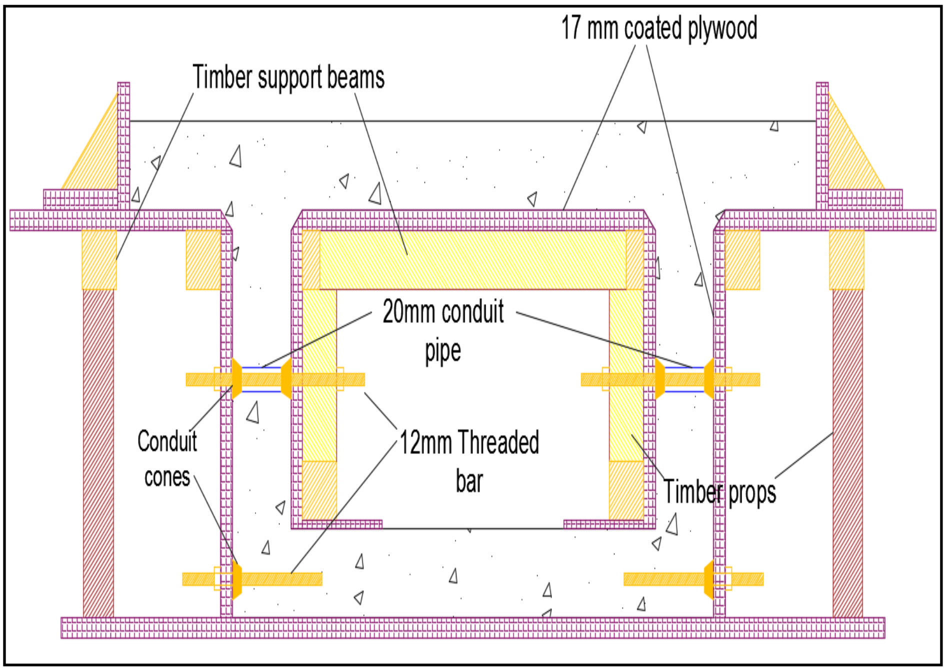

Figure 5. Formwork used during the constrcution [15, 16]

(a) *(b)*

Figure 6. Construction of the model,

Stage 1, (a) Before concreting, (b) After concreting

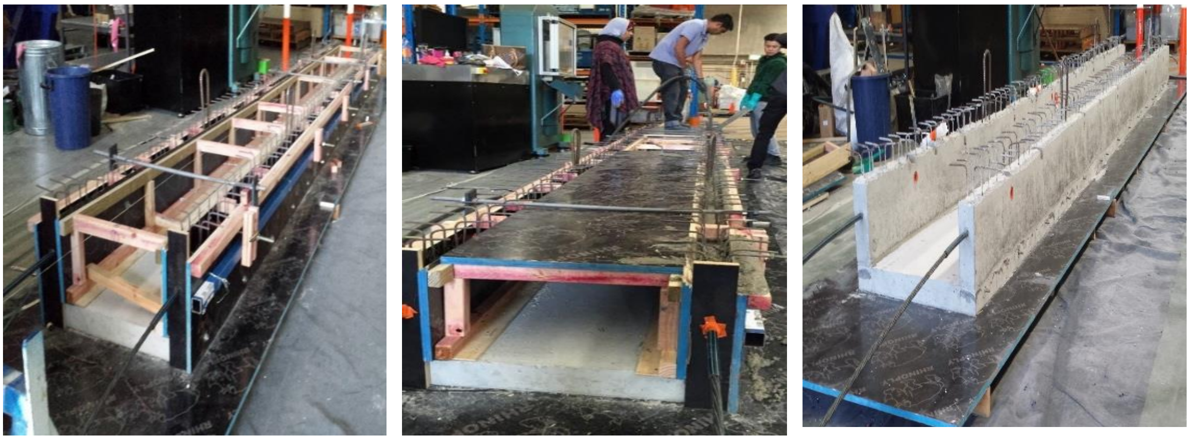

(a) *(c)* *(b)*

Figure 7. Construction of the model, Stage 2 (Webs), (a) Formwork for webs (b) Concreting the webs, (c) After removing formwork.

(a) (c) (b)

Figure 8. Construction of the model, Stage 3 (top slab)

(a) Reinforcing and formwork, (b) Top slab after concreting, (c) Completed model.

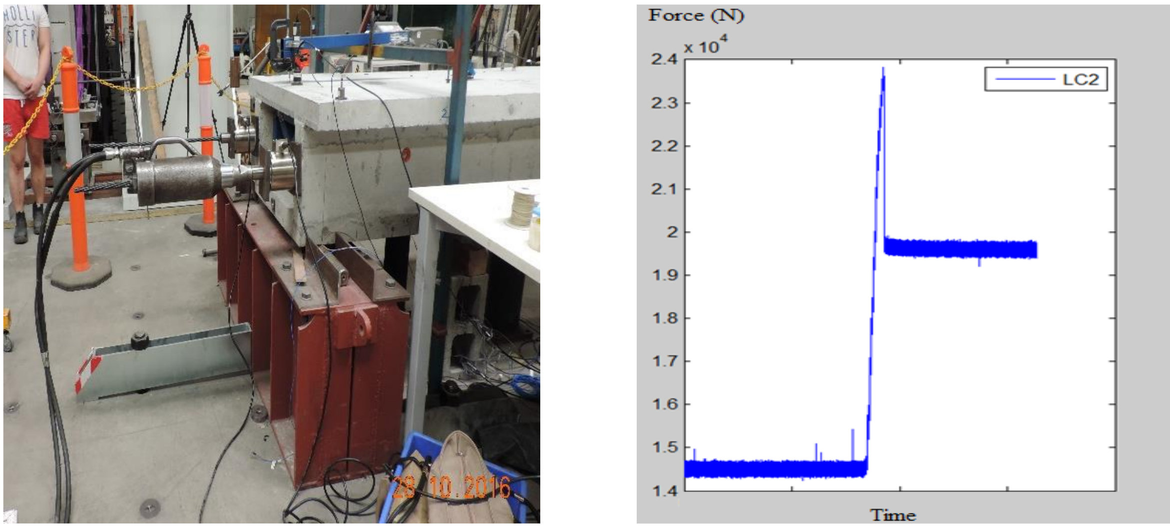

(a) (b)

Figure 9. Processs of appling the prestressed force, (a) Prestressing equipment and process, (b) Load cell reading during tensioning

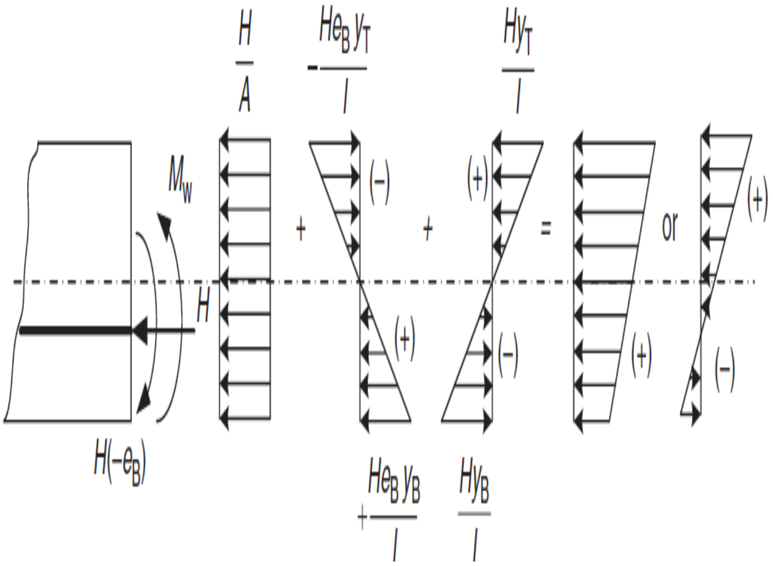

Figure 10. Stress distribution in prestressed box-girder beam under working load moment adapted from the Australian Standard AS 3600-2009 [23]

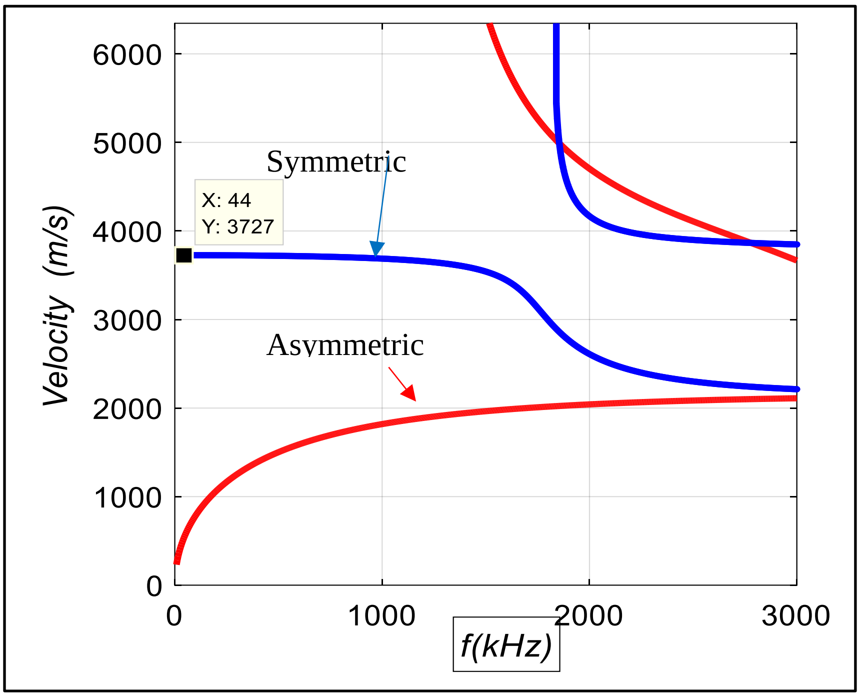

Figure 11. Ultrasonic wave phase velocity of the box-girder determined using WAVESCOPE software

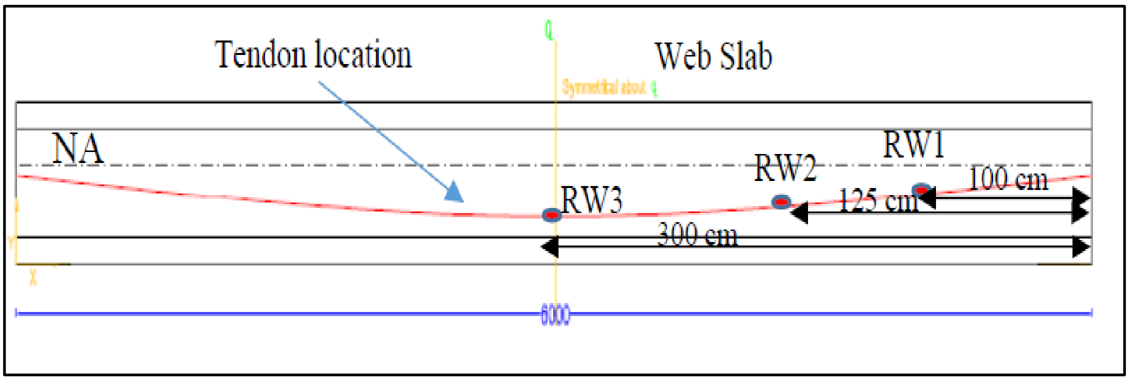

Figure 12. Positions of the receivers RW1, RW2 and RW3 on the web slab of the model (Note: the dimensions are not to scale).

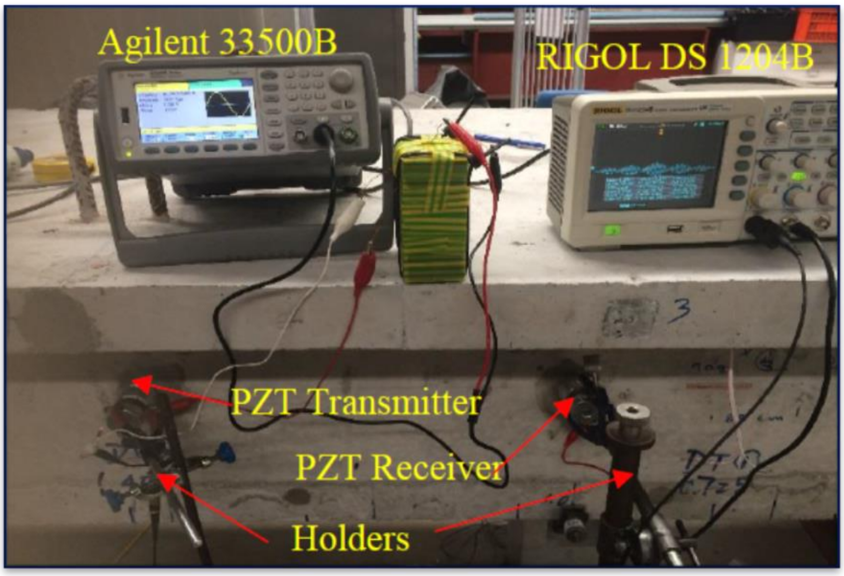

Figure 13. Test set-up at the web part of the box-girder.

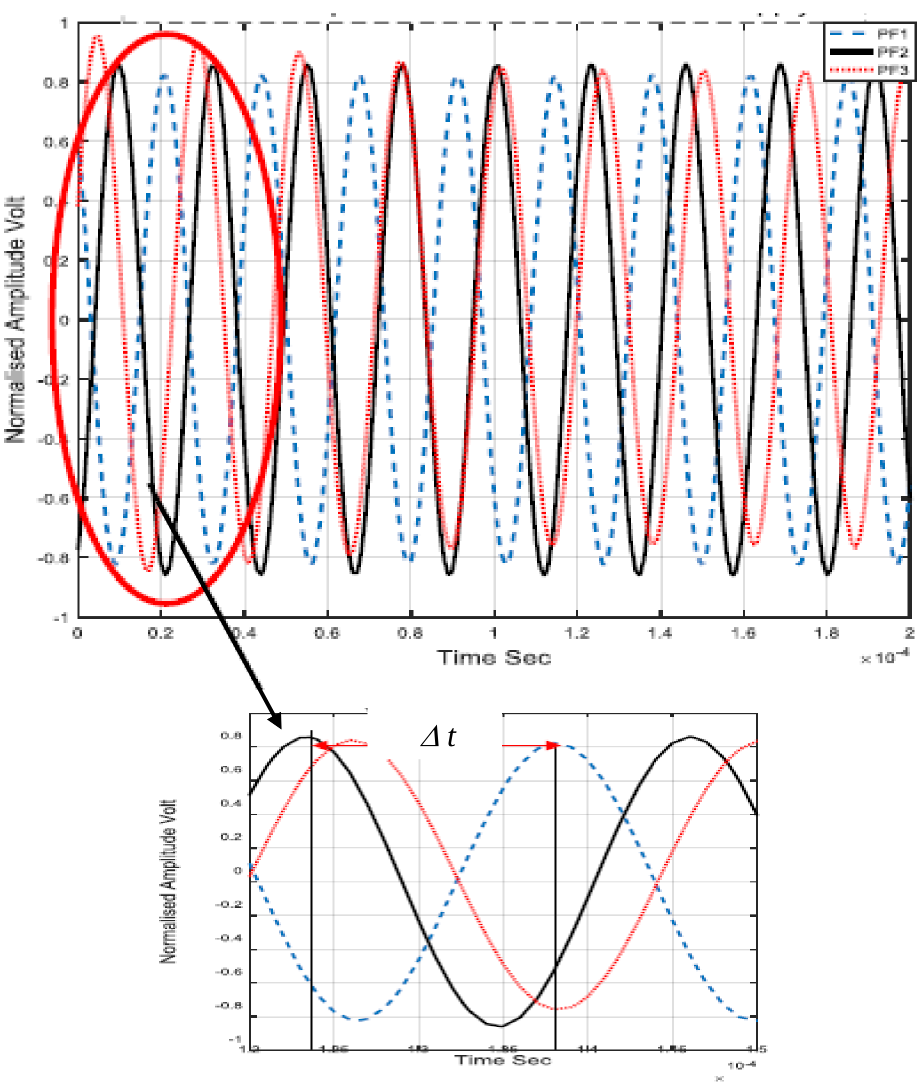

Figure 14. An example of signals received by RW1 with respect to different PF, with a close-up of the first part of the signal

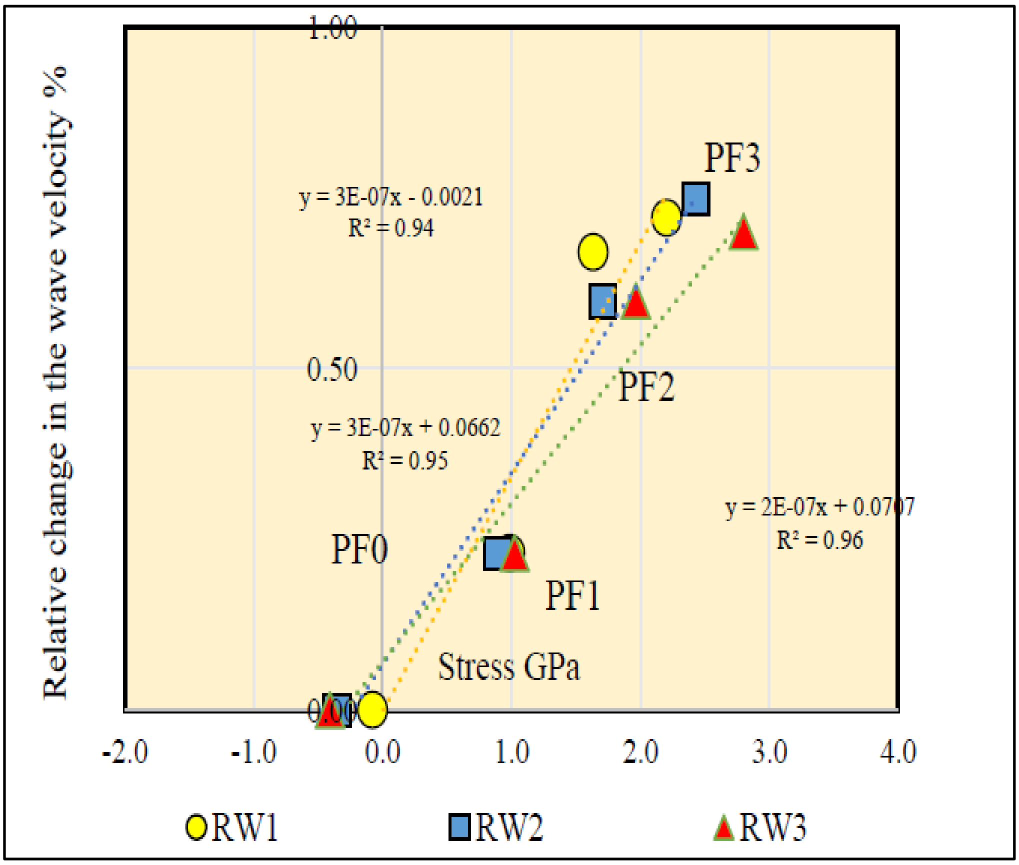

Figure 15. Relative changes in the wave velocity as a function of applied stress in the web slab of the model

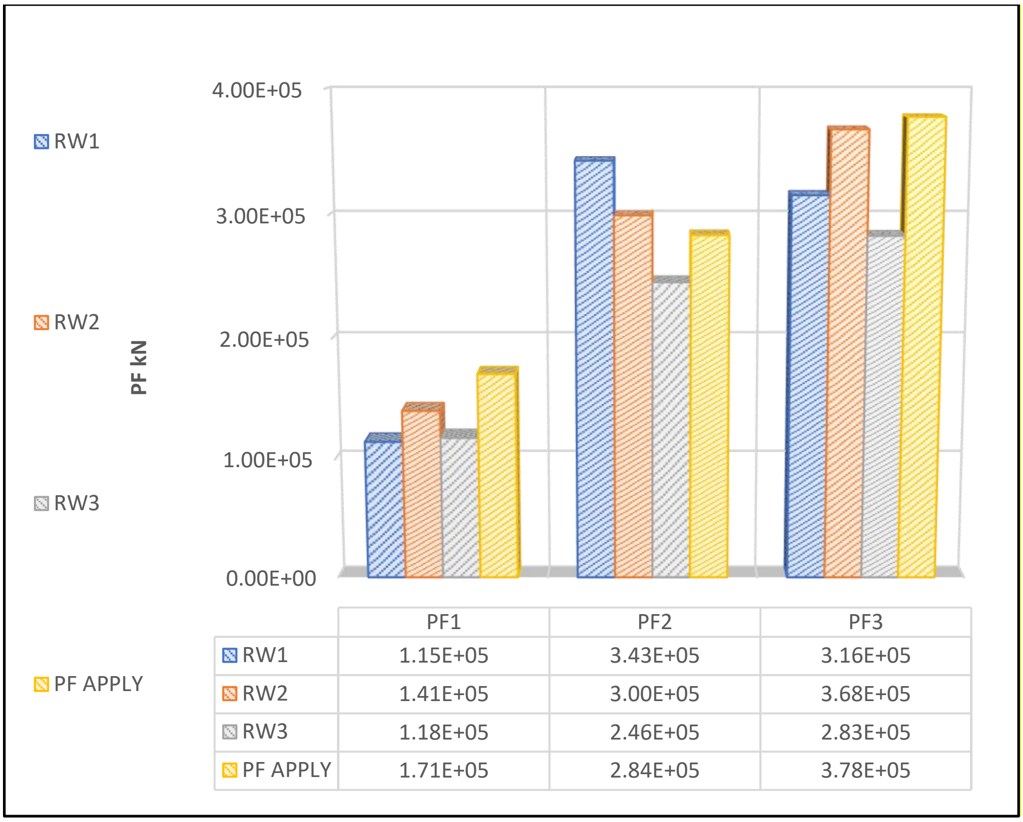

Figure 16. PF calculated from the ultrasonic wave data at the receiver's locations (web part results)

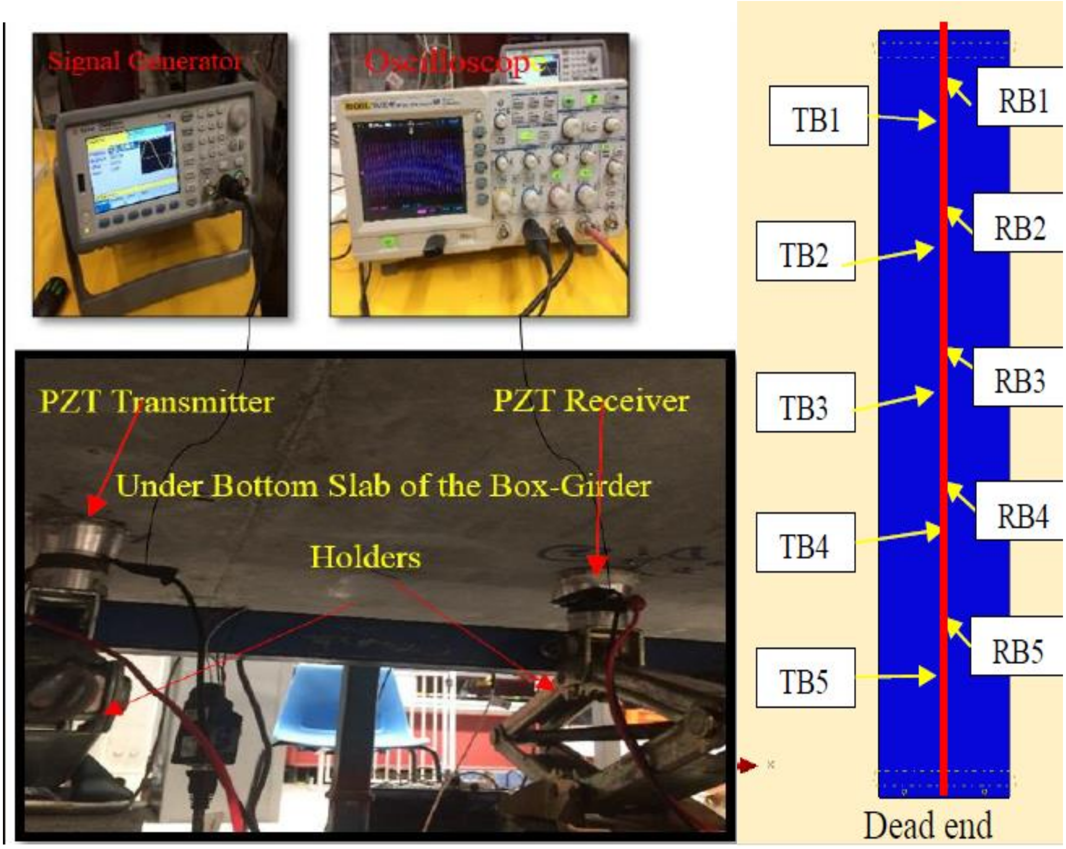

Figure 17. Experimental prototype with transducers placed under the bottom slab of the box-girder and the positions of the transmitters (TB) and the receivers(RB) under the bottom slab of the girder. (Note: the sketch is not to scale)

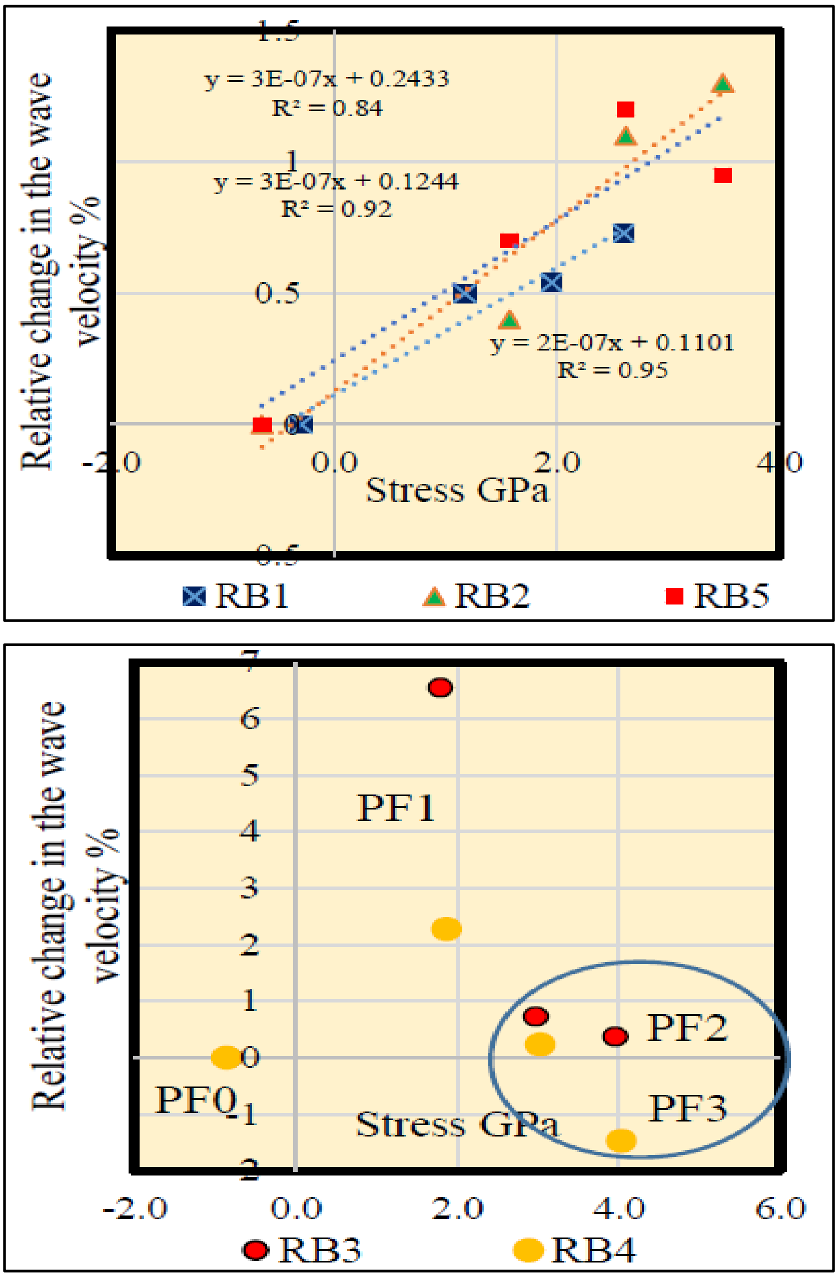

Figure 18. Relative change in the wave velocity as a function of applied stress of the receivers

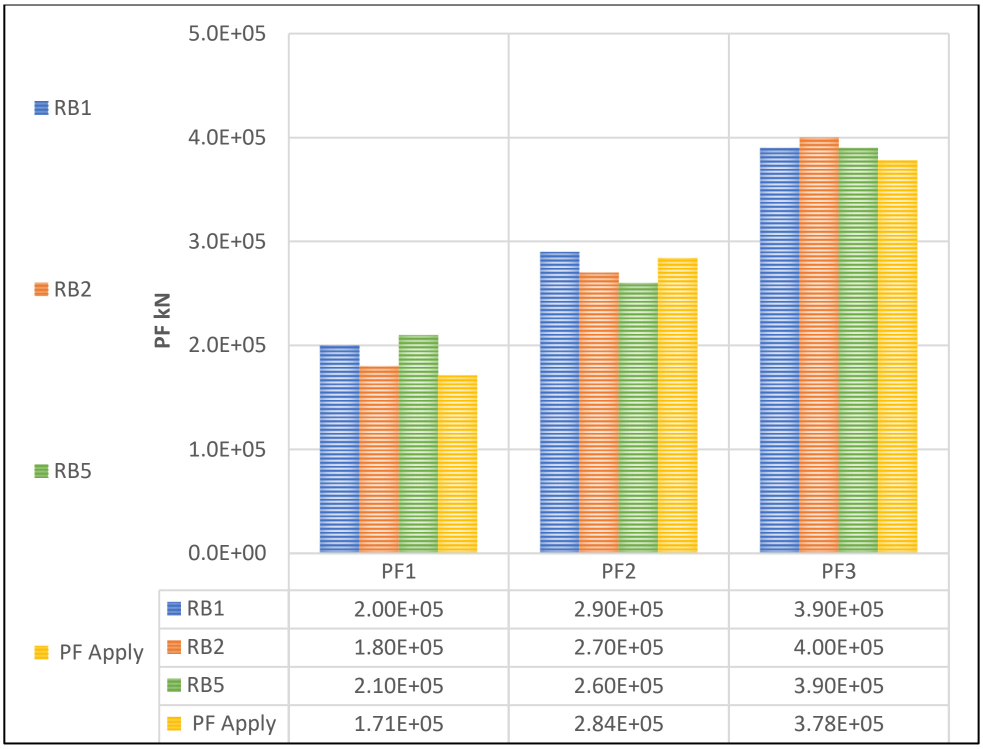

	PF1	PF2	PF3
RB1	2.00E+05	2.90E+05	3.90E+05
RB2	1.80E+05	2.70E+05	4.00E+05
RB5	2.10E+05	2.60E+05	3.90E+05
PF Apply	1.71E+05	2.84E+05	3.78E+05

Figure 19. Calculated PF from the ultrasonic wave data at the reciver's locations (under the bottom slab of the girder results)

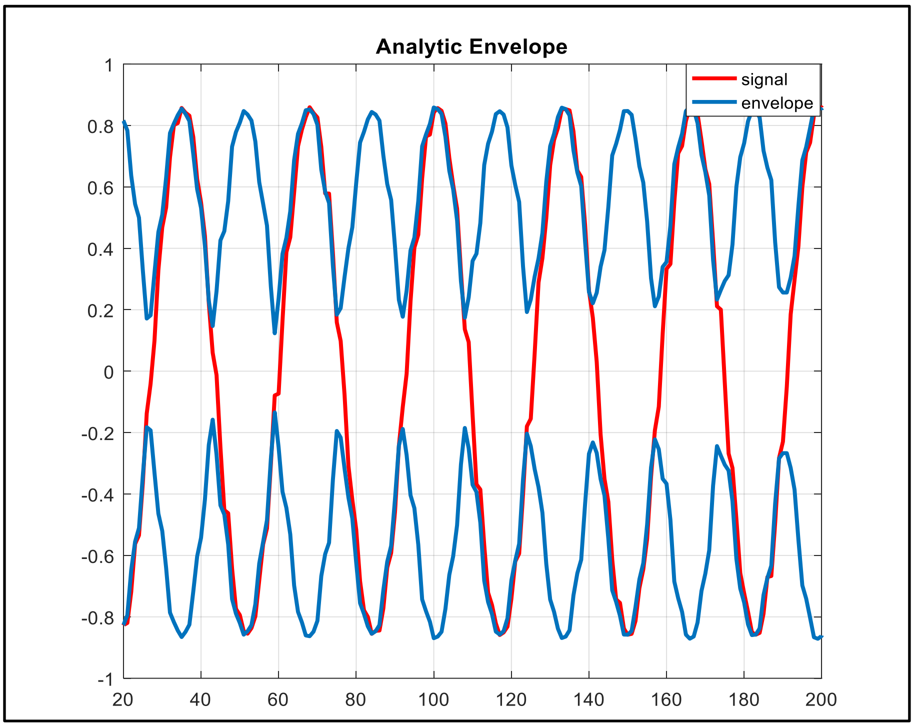

Figure 20. Received signal and the created energy envelope to calculate the area under the signal

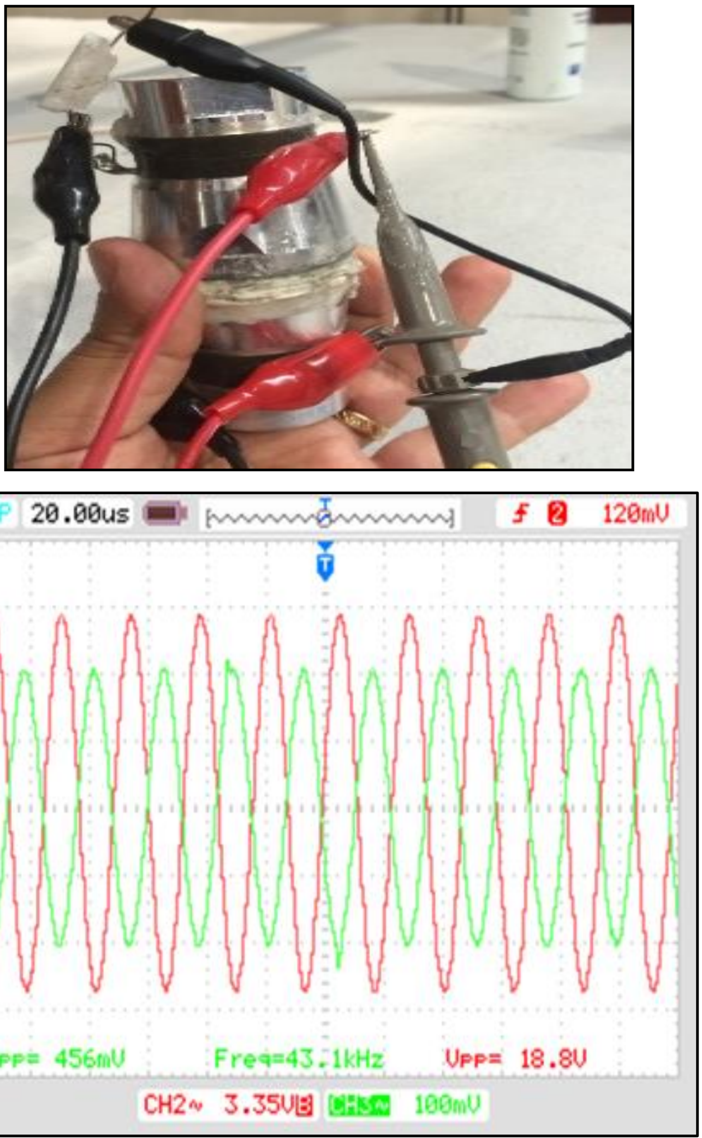

Figure 21. Measurement of the transmitted (face-to-face contact)

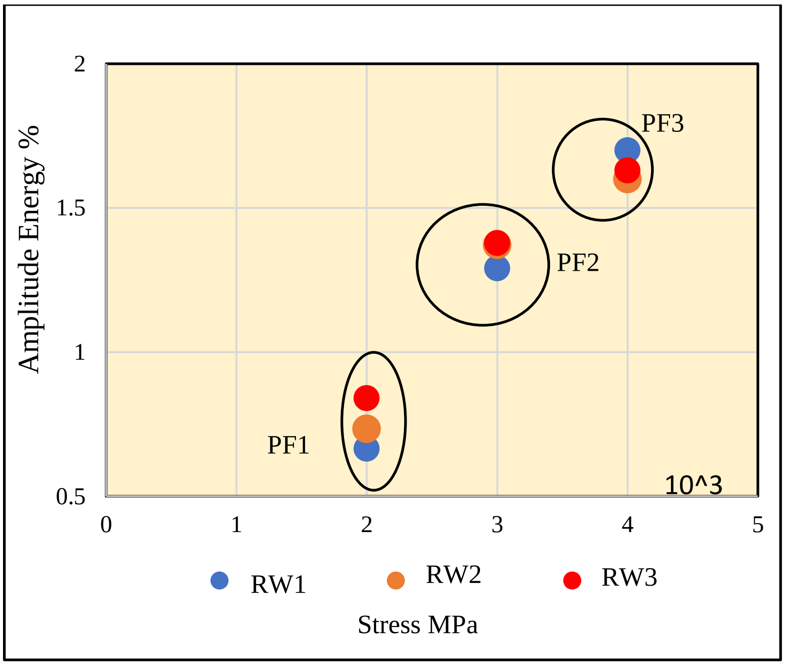

Figure 22. Waveform energy vs. stresses developed due to applying PF